Momentum Kick Model Description of the Ridge in $\Delta\phi$-$\Delta\eta$ Correlation in pp Collisions at 7 TeV[†]

Cheuk-Yin Wong

Physics Division, Oak Ridge National Laboratory, Oak Ridge, TN 37831
(Dated: May 31, 2011)

The near-side ridge structure in the $\Delta\phi$-$\Delta\eta$ correlation observed by the CMS Collaboration for pp collisions at 7 TeV at LHC can be explained by the momentum kick model in which the ridge particles are medium partons that suffer a collision with the jet and acquire a momentum kick along the jet direction. Similar to the early medium parton momentum distribution obtained in previous analysis for nucleus-nucleus collisions at 0.2 TeV, the early medium parton momentum distribution in pp collisions at 7 TeV exhibits a rapidity plateau as arising from particle production in a flux tube.

I. INTRODUCTION

Recently at LHC, the CMS Collaboration observed a $\Delta\phi$-$\Delta\eta$ correlation in pp collisions at $\sqrt{s_{NN}} = 7$ TeV [1], and in PbPb collisions at $\sqrt{s_{NN}} = 2.76$ TeV [2], where $\Delta\phi$ and $\Delta\eta$ are the azimuthal angle and pseudorapidity differences of two produced hadrons, respectively. The correlation appears in the form of a "ridge" that is narrow in $\Delta\phi$ at $\Delta\phi \sim 0$ and $\Delta\phi \sim \pi$, but relatively flat in $\Delta\eta$ (see Fig. 1(b) for pp high-multiplicity data below). Similar ridge structures have been observed previously in high-energy nucleus-nucleus AA collisions at RHIC by the STAR Collaboration [3–17], the PHENIX Collaboration [18–22], and the PHOBOS Collaboration [23], with or without a high-p_T trigger [4, 16, 24].

The CMS observations of the ridge in pp and PbPb collisions raise many interesting questions. How do the ridges arise in pp and AA collisions? Can the ridges in pp and PbPb collisions at LHC and in AA collisions at RHIC be described by the same physical phenomenon? If so, what are the similarities and differences? Why is the ridge yield greatest at $1 < p_T < 3$ GeV/c? What interesting physical quantities do the ridge data reveal? How are the ridges associated with a high-p_T trigger related to the ridges associated with autocorrelation without a high-p_T trigger?

Although many theoretical models have been proposed to discuss the ridge phenomenon in AA collisions [25–49] and pp collisions [49–62], the ridge phenomenon has not yet been fully understood. Most of the models deal only with some fragmented and qualitative parts of the experimental data. The most successful quantitative comparisons with experimental data have been carried out in the momentum kick model for the extensive sets of triggered associated particle data of the STAR Collaboration, the PHENIX Collaboration, and the PHOBOS

Collaboration — over large regions of p_t, $\Delta\eta$ and $\Delta\phi$ phase spaces, in many different phase space cuts and p_T combinations, including dependencies on centralities, dependencies on nucleus sizes, and dependencies on collision energies [25–27]. As it has been tried and tested successfully for AA collisions at RHIC in previous analyses from which a wealth of relevant pieces of information have been obtained, it is of interest to examine whether the momentum kick model can describe the CMS pp data at 7 TeV — to provide answers to the interesting questions we have just posed.

We shall first review the qualitative description of the momentum kick model in Section II. We then summarize the quantitative contents of the model in Section III. The determination of the centrality dependence of the ridge yield necessitates the evaluation of the number of kicked medium particles along the jet trajectory, which we describe in Section IV. Section V provides the numerical analysis of the ridge yield and the total associated particle distributions in pp collisions at 7 TeV, for comparison with the CMS data. In Section VI, we provide answers to the questions posed in the Introduction concerning the ridge phenomena in pp and AA collisions.

II. QUALITATIVE DESCRIPTION OF THE MOMENTUM KICK MODEL

Soon after the observation of the ridge effect in RHIC collisions, a momentum kick model was presented to explain the phenomenon [25–31]. In addition to providing a quantitative explanation of experimental data over large regions of p_t, $\Delta\eta$, and $\Delta\phi$ phase spaces in STAR, PHENIX, and PHOBOS experiments, the model serves the useful purposes of identifying and extracting important physical quantities that are otherwise difficult to measure.

To understand the physics of the ridge phenomenon, our first task is to ascertain what the correlated particles are. We need to specify the identities of the correlated particles for the case with a high p_t trigger as well as the autocorrelation case without a high p_t trigger. For
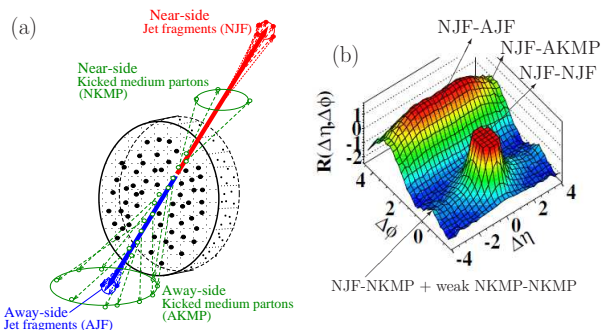
FIG. 1: (Color online) (a) Schematic representation of the momentum kick model. A jet pair (represented by thick arrows) occur back-to-back in a dense medium created in the collision. The jets collide with medium partons, lose energy, and fragment into near-side jet-fragments (NJF) and away-side jet-fragments (AJF). The near-side kicked medium partons (NMKP) and away-side kicked medium partons (AMKP) (represented by open circular points) that are kicked by the jets acquire a momentum kick along the jet directions and become correlated with the jets at $\Delta\phi \sim 0$ and $\Delta\phi \sim \pi$ as associated "ridge" particles. (b) The CMS data for high-multiplicity pp collisions at 7 TeV [1]. Different regions of the $\Delta\phi - \Delta\eta$ correlations may be identified as correlations of different particles associated with the jet fragments (JF) or kicked medium partons (KMP).

all cases the two detected particles are correlated in narrow azimuthal angles at $\Delta\phi \sim 0$ or at $\Delta\phi \sim \pi$, relative to each other. Such an experimental observation suggests that the correlated particles are related by a collision [25]. It is natural to consider the collision of jets with medium partons and attribute the ridge as arising from these direct collisions in the momentum kick model. Other models attribute the narrow $\Delta\phi$ correlations to other effects, and future investigations need to sort out the different consequences in quantitative comparison with experiment. Whatever the proposed mechanism may be, collisions of the jet with the medium partons are bound to occur, and the collisional correlation between the colliding objects as discussed in the momentum kick model must be taken into account.

In pp and AA collisions at high-energies, pairwise back-to-back jets are produced by the hard-scattering process. These jets encounter the dense medium that is also created in the collision. The jet that encounters lesser medium material is called the near-side jet. The other jet that encounters more medium material is the away-side jet, as depicted in Fig. 1(a). These two jets collide with medium partons, lose energy, and subsequently break up into jet fragments (JF) in the form of two narrow angular cones. The breakup of the near-side jet occurs most likely outside the medium. The away side is quenched. The location of the breakup of the away-side jet, if it is not completely quenched, depends on the degree of its quenching inside the dense medium. The medium partons have an initial momentum distribution at the moment of jet-(medium parton) collision. The kicked

medium partons (KMP) that are kicked by a jet acquire the additional momentum kick along the jet direction. Subsequently these kicked medium particles materialize as associated "ridge" particles to become correlated with the jets in the $\Delta\phi \sim 0$ and $\Delta\phi \sim \pi$ directions. The momentum distribution of the kicked medium particles will have a distribution that is given by the initial momentum distribution displaced by the momentum kick. As a consequence, related by jet-(medium parton) collisions are four types of particles. They are near-side and away-side jet fragments (JF) and near- and away-side kicked medium partons (KMP), as shown in Fig. 1(a).

In our attempt to identify the nature of the correlated particles, it is important to realize that the observed signals of correlations refer to those above an uncorrelated background, and the $\Delta\phi \sim 0$ and $\Delta\phi \sim \pi$ correlations place severe restrictions which are satisfied only by causally related particles. One can pick any two particles in random. If both particles arise from the bulk medium that are not related by collisions from the same jet pair as depicted in Fig. 1, the two-particle correlation will show up as a smooth background in which $\Delta\phi$ will be uniformly distributed. Such a smooth background has been subtracted from our consideration. The remaining correlation arises only from the portion of particles that are causally related by jet-(medium parton) collisions from the *same* pair of back-to-back jets.

Accordingly, we shall identify the two correlated particles as two of the four types of particles shown in Fig. 1(a). In the case with a triggered high-p_T jet particle, the triggered particle of the $\Delta\phi$-correlated pair can be identified as a near-side jet fragment (NJF). The other correlated particle can come from one of four possibilities:

1. **NJF-NJF Correlation**
   If the other particle is also a near-side jet fragment (NJF) from the fragmentation of the same near-side jet, they will be correlated in a cone at ($\Delta\phi \sim 0, \Delta\eta \sim 0$).

2. **NJF-NKMP Correlation**
   If the other particle is a near-side kicked medium parton (NKMP), the other particle will be distributed according to its initial momentum distribution displaced by the momentum kick. If the initial momentum distribution of the medium partons has a rapidity plateau, it will show up as a ridge along $\Delta\eta$ at $\Delta\phi \sim 0$.

3. **NJF-AKMP Correlation**
   If the other particle is an away-side kicked medium parton (AKMP), this particle will be distributed according to its initial momentum distribution displaced by the momentum kick. If the initial momentum distribution of the medium partons has a rapidity plateau, the kicked medium partons will show up as a ridge along $\Delta\eta$ at $\Delta\phi \sim \pi$. As there are more kicked medium partons on the away side than the near side, the ridge yield will be greater

on the away side than the ridge yield on the near side. Because of the increase in the final-state interactions after the medium partons are kicked, the $\Delta\phi$ and $\Delta\eta$ distributions are expected to be broadened. The degree of $\Delta\phi$ and $\Delta\eta$ broadening increases with the size of the colliding objects.

4. **NJF-AJF Correlation**

   If the other particle is a member of the away-side jet fragments (AJF), it will show up in a cone at $\Delta\phi \sim \pi$ and $\Delta\eta \sim 0$. Clearly, because of the multiple collisions with medium partons as the away-side jet passes through the medium, the jet becomes more broadly distributed in azimuthal and pseudo-rapidity angles. As a consequence, the away side jet fragments AJF correlated with the near-side jet has a broader distribution in $\Delta\phi$ and $\Delta\eta$, and a low average transverse momentum. The strength of the AJF will also be substantially quenched. The degree of broadening and quenching increases with the size of the colliding objects.

The $\Delta\phi$-$\Delta\eta$ correlation observed in pp collisions at 7 TeV by the CMS Collaboration contains these four distinct features listed above in high-multiplicity events, as indicated in Fig. 1(b).

It is important to note that the fragmentation of the degraded near-side jet produces not only high-p_t jet fragments but also low-p_t jet fragments. Evidence of the occurrence of low-p_T jet fragments in the fragmentation of a jet comes from a careful analysis of the two-particle correlation function of associated particle pairs down to p_t as low as 2-3 GeV/c [18]. From the angular cones of these particles as a function of the p_t of the correlated pair, one obtains useful systematics on the jet fragments as a function of p_t [29] (See Eqs. (7), (8), and (9) below). As p_T of the jet fragment decreases, the jet fragment number $\langle N_{\text{JF}} \rangle$ and the jet fragment temperature T_{JF} decreases, but the jet cone angular width of the jet fragments increases. The jet fragment number remain finite down to very low p_T, (even down to $p_T \to 0$) in the systematics. Another piece of evidence for the occurrence of low-p_T jet fragments comes from the autocorrelation measurements in STAR [4, 16, 24] where it was found that there are low p_T minijets (cluster of low-p_T particles) that are located at $(\Delta\phi \sim 0, \Delta\eta \sim 0)$ in excess of the background. These correlations arises from the fragmentation of a parent jet along the axis of the cone of these correlated pairs.

It should also be realized that the process of fragmentation of a near-side jet occurs most likely outside the medium as depicted in Fig. 1(a). These low p_T particles are subject to no final-state interactions with the medium. They can therefore preserve their correlations when they reach the detectors, resulting in the $(\Delta\eta \sim 0, \Delta\phi \sim 0)$ correlation peak as observed.

Because jet fragments can occur with both high and low p_T, we shall generalize the concept of "trigger" particles to include jet fragments of all p_T, both "high-p_T trigger" particles and low-p_T "self-triggered" particles.

Jet fragments from the same jet correlate with other jet fragments as part of a greater parent jet, no matter what the p_t values of these two jet fragments may be. They are the indicators of the presence of a parent jet. As indicators of a jet, they can be used as probes and reference markers to probe the correlation of other particles that have made collisions with the jet. By using such a generalized concept of "triggered" jet-particles of all p_T, the momentum kick model unifies the description of the observed "high-p_T triggered" ridge and the "low-p_T, self-triggered" ridge (which is sometimes also called soft ridge). It is not necessary to be a high-p_T particle to indicate the presence of a jet, low-p_T particles can also be a jet fragment and indicate the presence of a jet along the p_T direction, when they are used as correlation anchors to measure jet effects on other particles.

There is however a notable difference in the case of a high-p_T trigger and the case of autocorrelation without a high-p_T trigger. In the case with a high-p_T trigger, it is reasonable to take this trigger particle as a near-side jet fragment (NJF), and the near-side correlations come from its coincidence with another near-side jet fragment (NJF) or with a kicked medium parton (NKMP). The correlation contains the NJF-NJF and NJF-NKMP contributions only.

On the other hand, in the case of autocorrelation, one of the two correlated pair can be taken as a low-p_T "trigger" and the other as the associated particle. This low-p_T "trigger" particle can be either a near-side jet fragment (NJF) or a near-side kicked medium parton (NKMP). When this low-p_T particle comes from a jet fragment, this case of identifying this low-p_T particle as a jet fragment is not different from the case of a high-p_T trigger, and all earlier considerations can remain the same. However, when the low-p_T trigger is a near-side kicked medium parton (NKMP), there can be many additional contributions which we shall list below.

5. **NKMP-NKMP correlation**

   The associated particle can be a NKMP. There is thus an additional NKMP-NKMP contribution coming from the correlation of two near-side medium partons kicked by the same jet. Each of the kicked medium partons will lie within a small range of ϕ from the jet and therefore the two partons themselves will be correlated relative to each other, with $\Delta\phi \sim 0$. The width in $\Delta\phi$ in the NKMP-NKMP correlation is however wider than those of the NJF-NJF or NJF-NKMP correlations because it involve the folding of their $\Delta\phi$ correlations with the parent jet. If the initial momentum distribution of the medium partons has a rapidity plateau, the NKMP-NKMP correlations will show up at $\Delta\phi \sim 0$ as a ridge with a range that is twice longer than the ridge in the NJF-NKMP correlation.

6. **NKMP-AKMP correlation**

   If the low-p_T trigger is a near-side kicked medium

parton, the associated particle can be an away-side kicked medium parton. There is an additional NKMP-AKMP contribution to the two-particle correlation coming from the correlation of two medium partons kicked by a near-side jet and an away-side jet of the same parentage. The two kicked partons will be correlated relative to each other with $\Delta\phi \sim \pi$. If the initial momentum distribution of the two kicked partons has a rapidity plateau, then the NKMP-AKMP correlation will show up as a ridge along $\Delta\eta$ at $\Delta\phi \sim \pi$ with a range that is twice as long as the ridge in the NJF-NKMP correlation. The correlation may be attenuated and broadened because of the final-state interactions suffered by the AKMP after it is kicked by the away-side jet.

7. **NKMP-AJF correlation** If the low-p_T trigger is a near-side kicked medium parton and if the away-side jet is not completely quenched, the associated particle can be an away-side jet fragment. There is the additional NKMP-AJF contribution that shows up as a ridge along $\Delta\eta$ at $\Delta\phi \sim \pi$ with a range that is the same as the medium parton rapidity plateau.

From the above analysis, we can understand the relationship between the correlations in the case with a high-p_T trigger and in the case of autocorrelation involving low-p_T particles. If we consider the near-side, the case with a high-p_T trigger involves mainly NJF-NJF and NJF-NKMP correlations while the case of autocorrelations with low-p_T particles involves not only these NJF-NJF and NJF-NKMP correlations but also additional NKMP-NKMP. The NKMP-NKMP correlation will contribute only when more than one medium partons are kicked by the same jet and will be important in the ridge region. In extended dense medium as occurs in heavy-ion collisions, the number of partons kicked by the same jet becomes considerable and this NKMP-NKMP contribution should be appropriately taken into account. However, on the near-side in pp collisions, the number of medium partons kicked by the same jet is small, the NKMP-NKMP contribution is small in comparison with the other NJF-NJF and NJF-NKMP contributions, and can be approximately neglected.

III. QUANTITATIVE DESCRIPTION OF THE MOMENTUM KICK MODEL

Having presented a qualitative description of the momentum kick model, we turn now to the quantitative description of the model. To confine the scope of our investigation, we shall limit our attention to the correlation of near-side particles. We shall neglect the NKMP-NKMP contribution, which is a valid consideration for pp collisions that involve only a small number of medium partons kicked by the same parent jet.

We briefly summarize the main quantitative contents of the momentum kick model as described in detail in [25–31]. We follow a jet as it collides with medium partons in a dense medium and study the yield of associated particles for a given p_t^{trig} which has been generalized to include cases of all p_T, as providing an angular location marker for the parent jet.

We label the normalized initial medium parton momentum distribution at the moment of jet-(medium parton) collisions by $E_i dF/d\mathbf{p}_i$. The jet imparts a momentum $\mathbf{q}$ onto a kicked medium parton, which changes its momentum from $\mathbf{p}_i$ to $\mathbf{p} = (p_t, \eta, \phi) = \mathbf{p}_i + \mathbf{q}$, as a result of the jet-(medium parton) collision. By assumption of parton-hadron duality, the kicked medium partons subsequently materialize as observed associated ridge hadrons.

The normalized final parton momentum distribution $E dF/d\mathbf{p}$ at $\mathbf{p}$ is related to the normalized initial parton momentum distribution $E_i dF/d\mathbf{p}_i$ at $\mathbf{p}_i$ at a shifted momentum, $\mathbf{p}_i = \mathbf{p} - \mathbf{q}$, and we have [25–31]

$$\frac{dF}{p_t dp_t d\eta d\phi} = \left[\frac{dF}{p_{ti} dp_{ti} dy_i d\phi_i}\frac{E}{E_i}\right]_{\mathbf{p}_i = \mathbf{p} - \mathbf{q}}$$
$$\times \sqrt{1 - \frac{m^2}{(m^2 + p_t^2)\cosh^2 y}}, \qquad (1)$$

where the factor E/E_i ensures conservation of particle numbers and the last factor changes the rapidity distribution of the kicked partons to the pseudorapidity distribution [63]. Changing the angular variables to $\Delta\eta = \eta - \eta^{\mathrm{trig}}$, $\Delta\phi = \phi - \phi^{\mathrm{trig}}$ and characterizing the number of partons kicked by the jet (per jet) by $\langle N_k \rangle$, we obtain the charged ridge particle momentum distribution per trigger jet as

$$\left[\frac{dN_{\mathrm{ch}}}{N_{\mathrm{trig}} p_t dp_t d\Delta\eta d\Delta\phi}\right]_{\mathrm{ridge}} = f_R \frac{2}{3}\langle N_k \rangle\left[\frac{dF}{p_{ti} dp_{ti} dy_i d\phi_i}\frac{E}{E_i}\right]_{\mathbf{p}_i = \mathbf{p} - \mathbf{q}}$$
$$\times \sqrt{1 - \frac{m^2}{(m^2 + p_t^2)\cosh^2 y}}, \qquad (2)$$

where f_R is the average survival factor for produced ridge particles to reach the detector, and the factor $2/3$ is to indicate that $2/3$ of the produced associated particles are charged. Present measurements furnish information only on the product $f_R\langle N_k \rangle$. For pp collisions with a small transverse extension, the kicked medium partons are likely to escape from the interaction region after the kick and f_R can be approximately taken to be unity. The momentum kick $\mathbf{q}$ will be distributed in the form of a cone around the trigger jet direction with an average $\langle\mathbf{q}\rangle = q_L \mathbf{e}^{\mathrm{trig}}$ directed along the trigger direction $\mathbf{e}^{\mathrm{trig}}$ of the parent jet.

We have extracted the normalized initial medium parton momentum distribution on the right hand side of Eq. (2) from STAR, PHENIX, and PHOBOS data, we find that the distribution can be represented in the form [26–

31]

$$\frac{dF}{p_{ti}dp_{ti}dy_id\phi_i} = A_{\rm ridge}(1-x)^a\frac{e^{-\sqrt{m_\pi^2+p_{ti}^2}/T_{\rm MP}}}{\sqrt{m_d^2+p_{ti}^2}}, (3)$$

where $A_{\rm ridge}$ is a normalization constant, x is the light-cone variable

$$x = \frac{\sqrt{m_\pi^2+p_{ti}^2}}{m_\pi}e^{|y_i|-y_B}, (4)$$

a is the fall-off parameter, y_B is the rapidity of the beam nucleons in the CM system, T_{MP} is the medium parton temperature parameter, m_π is the pion mass, and $m_d = 1$ GeV is to correct for the behavior of the p_T distribution at low p_T.

The total observed yield of associated particles per trigger consists of the sum of the ridge (NJF-NKMP) component and the jet fragments (NJF-NJF) component,

$$\left[\frac{1}{N_{\rm trig}}\frac{dN_{\rm ch}}{p_tdp_td\Delta\eta d\Delta\phi}\right]_{\rm total} = \left[\frac{dN_{\rm ch}}{N_{\rm trig}p_tdp_td\Delta\eta\,d\Delta\phi}\right]_{\rm ridge}$$

$$+f_J\left[\frac{dN_{\rm jet}^{pp}}{p_tdp_t\,d\Delta\eta\,d\Delta\phi}\right]_{\rm JF}, (5)$$

where f_J is the survival factor of the jet fragments as they propagate out of the medium. For fragmentation outside the medium, as is likely to occur in pp collisions, f_J can be set to unity. The experimental associated jet fragment distribution in pp collisions can be described well by [28]

$$\left[\frac{dN_{\rm JF}^{pp}}{p_tdp_t\,d\Delta\eta\,d\Delta\phi}\right]_{\rm JF} = N_{\rm JF}\frac{\exp\{(m_\pi-\sqrt{m^2+p_t^2})/T_{\rm JF}\}}{T_{\rm JF}(m_\pi+T_{\rm JF})}$$

$$\times\frac{1}{2\pi\sigma_\phi^2}e^{-[(\Delta\phi)^2+(\Delta\eta)^2]/2\sigma_\phi^2}, (6)$$

where $N_{\rm JF}$ is the total number of near-side (charged) jet fragments associated with the p_T trigger and $T_{\rm JF}$ is the jet fragment temperature parameter. Extensive sets of data from the PHENIX Collaboration give $N_{\rm JF}$ and $T_{\rm JF}$ parameters that vary approximately linearly with $p_t^{\rm trig}$ of the "trigger" particle for pp collisions at 0.2 TeV [27],

$$N_{\rm JF} = 0.15 + (0.06/{\rm GeV/c})\,p_t^{\rm trig}, (7)$$

$$T_{\rm JF} = 0.19\text{ GeV} + 0.06\,p_t^{\rm trig}. (8)$$

We also find that the width parameter σ_ϕ of the jet fragment cone depends slightly on p_t which we parametrize as

$$\sigma_\phi = \sigma_{\phi 0}\frac{m_a}{\sqrt{m_a^2+p_t^2}}, (9)$$

where $m_a = 1.1$ GeV.

With the above formulation, the associated particle distribution is written in terms of physical quantities, namely, the initial medium parton momentum distribution $EdF/d\boldsymbol{p}$, the magnitude of the momentum kick q_L, and the number of kicked medium particles $\langle N_k\rangle$ which depends on the centrality of the collision.

IV.   CENTRALITY DEPENDENCE OF THE RIDGE YIELD

The CMS collaboration obtained the ridge yield as a function of the charge multiplicity. It is necessary to determine the centrality dependence of both the ridge yield and the charge multiplicity.

In the momentum kick model, the ridge yield is proportional to the number of kicked medium partons. We show previously how the (average) number of kicked medium partons per jet, $\langle N_k(\boldsymbol{b})\rangle$, can be evaluated as a function of the impact parameter $\boldsymbol{b}$ for AA collisions [28, 29] . Here, we briefly summarize these results and apply them to pp collisions by treating the colliding protons as extended droplets as in the Chou-Yang model [64].
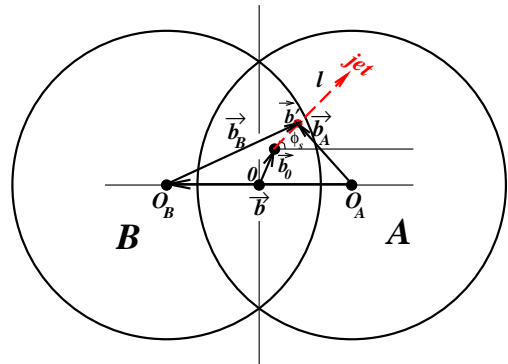

FIG. 2:   (Color online) The transverse coordinate system used to calculate the number of kicked medium partons along the jet trajectory in the collision of A and B at an impact parameter $\boldsymbol{b} = \boldsymbol{b}_A - \boldsymbol{b}_B$. The jet source point is $\boldsymbol{b}_0$ and the jet-(medium parton) collision point is $\boldsymbol{b}'$. The jet trajectory lies along $\boldsymbol{l}$ and makes an angle ϕ_s with respect to the reaction plane.

Accordingly, we examine the collision of two extended objects A and B in Fig. 2 and use the transverse coordinate system with the origin at $\boldsymbol{O}$ that is the midpoint between the two centers, $\boldsymbol{O}_A$ and $\boldsymbol{O}_B$, of the extended objects. In this transverse coordinate system, the location of the jet production point is labeled as $\boldsymbol{b}_0$, measured from the origin $\boldsymbol{O}$. The jet is produced by the collision of a projectile-nucleon parton and a target-nucleon parton at $\boldsymbol{b}_0$. The jet production point $\boldsymbol{b}_0$ measured relative to the two nucleon centers $\boldsymbol{O}_A$ and $\boldsymbol{O}_B$ are then given by

$$\boldsymbol{b}_A = \boldsymbol{b}_0 + \boldsymbol{b}/2, (10)$$

$$\boldsymbol{b}_B = \boldsymbol{b}_0 - \boldsymbol{b}/2. (11)$$

From the Glauber model, the probability of finding a target parton at $\boldsymbol{b}_0$ is $T_A(\boldsymbol{b}_A)$, and the probability of finding a projectile parton at $\boldsymbol{b}_0$ is $T_B(\boldsymbol{b}_B)$. The probability for the production of a jet at $\boldsymbol{b}_0$ in the collision of A and B at an impact parameter $\boldsymbol{b}$, $P_{\rm jet}(\boldsymbol{b}_0,\boldsymbol{b})$, is

$$P_{\rm jet}(\boldsymbol{b}_0,\boldsymbol{b}) = \frac{T_A(\boldsymbol{b}_0+\boldsymbol{b}/2)T_B(\boldsymbol{b}_0-\boldsymbol{b}/2)}{\int d\boldsymbol{b}_0 T_A(\boldsymbol{b}_0+\boldsymbol{b}/2)T_B(\boldsymbol{b}_0-\boldsymbol{b}/2)}, (12)$$

which is normalized as

$$\int d\boldsymbol{b}_0 P_{\mathrm{jet}}(\boldsymbol{b}_0, \boldsymbol{b}) = 1. \tag{13}$$

We consider the near-side jet to traverse along the trajectory $\boldsymbol{l}$ which is measured from the point of production $\boldsymbol{b}_0$ and points in the ϕ_s direction with respect to the reaction plane, as shown in Fig. 2. The jet will collide with medium partons along its way. We consider one such a collision at the transverse coordinate $\boldsymbol{b}'$ as measured from the origin $\boldsymbol{O}$. The collision point $\boldsymbol{b}'_A$ and $\boldsymbol{b}'_B$ measured relative to the two centers $\boldsymbol{O}_A$ and $\boldsymbol{O}_B$ are then given by

$$\boldsymbol{b}'_A = \boldsymbol{b}' + \boldsymbol{b}/2, \tag{14}$$
$$\boldsymbol{b}'_B = \boldsymbol{b}' - \boldsymbol{b}/2, \tag{15}$$
$$\boldsymbol{b} = \boldsymbol{b}'_A - \boldsymbol{b}'_B. \tag{16}$$

The collision point $\boldsymbol{b}'$ depend on $\boldsymbol{b}_0$, $\boldsymbol{l}$, and ϕ_s as given by

$$\boldsymbol{b}'(\boldsymbol{b}_0, \boldsymbol{l}, \phi_s) = (b'_x, b'_y) = (b_{0x} + l\cos\phi_s, b_{0y} + l\sin\phi_s) \tag{17}$$

which will be needed later on to evaluate the number of kicked medium partons. We label the number of kicked medium partons per jet as $N_k(\boldsymbol{b}_0, \phi_s, \boldsymbol{b})$. The average of $N_k(\boldsymbol{b}_0, \phi_s, \boldsymbol{b})$ with respect to $\boldsymbol{b}_0$ is

$$\begin{aligned}\bar{N}_k(\phi_s, \boldsymbol{b}) &\equiv \langle N_k(\boldsymbol{b}_0, \phi_s, \boldsymbol{b})\rangle_{\boldsymbol{b}_0} \\ &= \frac{\int d\boldsymbol{b}_0 N_k(\boldsymbol{b}_0, \phi_s, \boldsymbol{b}) P_{\mathrm{jet}}(\boldsymbol{b}_0, \boldsymbol{b})}{\int d\boldsymbol{b}_0 P_{\mathrm{jet}}(\boldsymbol{b}_0, \boldsymbol{b})}. \end{aligned} \tag{18}$$

The jet is attenuated along its way, and the attenuation is described by $\exp\{-\zeta N_k(\boldsymbol{b}_0, \phi_s, \boldsymbol{b})\}$ with an attenuation coefficient ζ that depends on the energy loss and the change of the fragmentation function on energy [27]. So when the jet attenuation is taken into account, we get

$$\begin{aligned}\bar{N}_k(\phi_s, \boldsymbol{b}) &\equiv \langle N_k(\boldsymbol{b}_0, \phi_s, \boldsymbol{b})\rangle_{\boldsymbol{b}_0} \\ &= \frac{\int d\boldsymbol{b}_0 N_k(\boldsymbol{b}_0, \phi_s, \boldsymbol{b}) e^{-\zeta N_k(\boldsymbol{b}_0, \phi_s, \boldsymbol{b})} P_{\mathrm{jet}}(\boldsymbol{b}_0, \boldsymbol{b})}{\int d\boldsymbol{b}_0 e^{-\zeta N_k(\boldsymbol{b}_0, \phi_s, \boldsymbol{b})} P_{\mathrm{jet}}(\boldsymbol{b}_0, \boldsymbol{b})}. \end{aligned} \tag{19}$$

We further get the average over angle ϕ_s and we get

$$\begin{aligned}\bar{\bar{N}}_k(\boldsymbol{b}) &\equiv \langle N_k(\boldsymbol{b}_0, \phi_s, \boldsymbol{b})\rangle_{\boldsymbol{b}_0, \phi_s} \\ &= \frac{1}{\pi/2} \int_0^{\pi/2} d\phi_s \langle N_k(\boldsymbol{b}_0, \phi_s, \boldsymbol{b})\rangle_{\boldsymbol{b}_0}. \end{aligned} \tag{20}$$

To proceed further, we need to evaluate $N_k(\boldsymbol{b}_0, \phi_s, \boldsymbol{b})$. The number of jet-(medium parton) collisions along the jet trajectory that originates from $\boldsymbol{b}_0$ and makes an angle ϕ_s with respect to the reaction plane is

$$N_k(\boldsymbol{b}_0, \phi_s, \boldsymbol{b}) = \int_0^\infty \sigma \, dl \frac{dN_{\mathrm{MP}}}{dV}(\boldsymbol{b}'_A, \boldsymbol{b}'_B), \tag{21}$$

where $0 < l < \infty$ parametrizes the jet trajectory, σ is the jet-(medium parton) scattering cross section, and

$dN_{\mathrm{MP}}(\boldsymbol{b}')/dV$ is the medium parton density at $\mathbf{b}'$ along the trajectory $\boldsymbol{l}$. We start the time clock for time measurement at the moment of maximum overlap of the colliding nuclei, and the jet is produced by (nucleon parton)-(nucleon parton) collisions at a time $t \sim \hbar/(10 \text{ GeV})$ which can be taken to be ~ 0. The trajectory path length l is then a measure of the time coordinate, $t \approx l$. Due to the longitudinal expansion the density is depleted and the temperature is decreased as [72]

$$T \propto (t_0/t)^{c_s^2}, \tag{22}$$

where c_s is the speed of sound and t_0 is the initial time. As the entropy density and number densities are proportional to T^{1/c_s^2}, the density of the medium partons therefore varies with time t as [72]

$$\frac{dN_{\mathrm{MP}}}{dV}(b', t) = \frac{dN_{\mathrm{MP}}}{dV}(b', t = t_0)\frac{t_0}{t}. \tag{23}$$

The medium parton density dN_{MP}/dV at $(b'_{\mathrm{init}}, t = t_0)$ is related to the parton transverse density $dN_{\mathrm{MP}}/d\boldsymbol{b}$ at t_0 by

$$\frac{dN_{\mathrm{MP}}}{dV}(b', t = t_0) = \frac{dN_{\mathrm{MP}}}{2t_0 d\boldsymbol{b}'}(b', t = t_0). \tag{24}$$

To obtain the medium parton density, we introduce the concept of an extended droplet to describe the proton, as in the Chou-Yang [64] model with the droplet number of a proton normalized to unity. Collisions between droplet elements of one proton and the droplet elements of the other proton leads to the production the medium partons. As in high-energy heavy-ion collision, we assume that the number of medium partons is proportional to the number of participating droplet elements N_{particp} with a proportional constant κ'

$$\frac{dN_{\mathrm{MP}}}{dN_{\mathrm{particp}}} = \kappa'. \tag{25}$$

The initial parton number transverse density $dN_{\mathrm{MP}}/d\boldsymbol{b}'$ at $t = t_0$ is then related to the corresponding participating droplet element transverse density $dN_{\mathrm{MP}}/d\boldsymbol{b}'$ as

$$\frac{dN_{\mathrm{MP}}}{d\boldsymbol{b}'} = \kappa'\frac{dN_{\mathrm{particp}}}{d\boldsymbol{b}'}. \tag{26}$$

We need to evaluate the κ' parameter for pp collision at 7 TeV. Landau hydrodynamical model gives [66–68]

$$N_{\mathrm{ch}} = K(\xi\sqrt{s_{NN}}/\text{GeV})^{1/2}, \tag{27}$$

where $K = 2.019$ and ξ is the fraction of incident energy that goes into particle production in pp and $p\bar{p}$ collisions. A examination of the charge multiplicity in pp and $p\bar{p}$ collisions indicates that the particle production energy fraction ξ is approximately 0.5 for these collisions [69]. So, for pp at 7 GeV, the average charge multiplicity is

$$N_{\mathrm{ch}} = 120. \tag{28}$$

To determine κ', we use a sharp-cutoff thickness function of the form for the nucleons, Eq. (12.29)

$$T_A(\boldsymbol{b}_A) = \frac{3}{2\pi R_A^3}\sqrt{R_A^2 - b_A^2} \;\; \Theta(R_a - b_A), \qquad (29)$$

which gives an average number of participating droplet elements $\langle N_{\text{particp}} \rangle = 0.4894$ and

$$\frac{N_{\text{MP}}}{N_{\text{particp}}} = \frac{dN_{\text{MP}}}{dN_{\text{particp}}} = \frac{3}{2}\frac{dN_{\text{ch}}}{dN_{\text{particp}}} = \kappa' = 367. \quad (30)$$

The transverse participant number density needed in Eqs. (21) and (26) along the jet trajectory can be obtained from the Glauber model to be

$$\frac{dN_{\text{particp}}}{d\boldsymbol{b}'}(\boldsymbol{b}'_A, \boldsymbol{b}'_B) = [T_A(\boldsymbol{b}'_A) + T_B(\boldsymbol{b}'_B)] \; \Theta(\mathcal{R}), \quad (31)$$

where $\Theta(\mathcal{R})$ denotes a step function that is unity inside the overlapping region and zero outside. The number of jet-(medium parton) collisions along the jet trajectory making an angle ϕ_s with respect to the reaction plane is

$$N_k(\boldsymbol{b}_0, \phi_s, \boldsymbol{b}) = \int_0^\infty \frac{\sigma \, dl}{2t_0} \kappa' \left[T_A(\boldsymbol{b}'_A) + T_B(\boldsymbol{b}'_B) \right] \Theta(\mathcal{R}) \frac{t_0}{t} (32)$$

where $\boldsymbol{b}'_A$ and $\boldsymbol{b}'_B$ are given in terms of $\boldsymbol{b}_0, \phi_s, \boldsymbol{b}$ and $\boldsymbol{l}$ by Eqs. (14), (15), and (17). This expression allows us to evaluate the number of average kicked medium partons per jet $\bar{\bar{N}}(\boldsymbol{b})$ as a function of the impact parameter.

There is an amendment which need to be taken into account. To produce a medium parton with a transverse mass $m_T \sim p_T$, a period of initial time $t_0 \sim \hbar/p_T$ is however needed to convert the longitudinal kinetic energy of the collision into entropy so that the jet-MP collision can commence [72]. At RHIC with $\sqrt{s_{NN}} =$ of 0.2 TeV, the time for producing a particle with a typical transverse mass or transverse momentum of about 0.35 GeV is $\hbar/(0.35 \text{ GeV/c}) \sim 0.6$ fm/c, which is also the time estimated for the thermalization of the produced matter [70]. Previous estimates of the jet-MP cross section and attenuation coefficient ζ have been obtained with such a t_0 value. At LHC with $\sqrt{s_{NN}} =$ of 7 TeV, $\langle p_T \rangle = 0.545$ GeV/c [75], which is substantially greater than the average transverse momentum in RHIC collisions at 0.2 TeV. Consequently, we need a smaller value of t_0 for LHC collisions as compared to RHIC collisions.

Equation (32) can be substituted into Eq. (20) to allow the evaluation of the number of ridge particles $\bar{\bar{N}}_k(\boldsymbol{b})$ as a function of the impact parameter b.

We also need the relation between the charge multiplicity $N_{\text{ch}}(\boldsymbol{b})$ inside the CMS rapidity window as a function of the impact parameter $\boldsymbol{b}$. Using Eqs. (30) and (31), we obtain

$$N_{\text{ch}}(\boldsymbol{b})$$
$$= C_{\text{CMS}}\frac{2}{3}\kappa' \int d\boldsymbol{b}'[T_A(\boldsymbol{b}' + \boldsymbol{b}/2) + T_B(\boldsymbol{b}' - \boldsymbol{b}/2)]\Theta(\mathcal{R}),$$
$$(33)$$

where C_{CMS} is the fraction of produced particles inside the CMS rapidity window of $-2.4 < \eta < 2.4$. Assuming a rapidity plateau for produced particles, this fraction for the multiplicity of particles, within the CMS rapidity window in pp collisions 7 TeV with $y_B = 8.91$, is

$$C_{\text{CMS}} = \frac{(\text{CMS rapidity range})}{2y_B} = 0.269. \qquad (34)$$

By using these results, we can relate the CMS charge multiplicity $N_{\text{ch}}(\boldsymbol{b})$ and the average number of kicked medium partons $\bar{\bar{N}}_k(\boldsymbol{b})$.

V. MOMENTUM KICK MODEL ANALYSIS OF pp COLLISIONS AT 7 GEV

Previously, the momentum kick model analyses of STAR, PHENIX and PHOBOS data yield a wealth of useful information. We learn that the initial momentum distribution is in the form of a rapidity plateau, as in the production of particles in a flux tube [30, 63, 71–73], and the transverse distribution is in the form of a thermal-type distribution with a medium-parton temperature T_{MP}. The STAR ridge data at 0.2 TeV can be described by a medium parton (MP) momentum distribution of the form in Eq. (3) with parameters [26–30]

$$a = 0.5, \;\; T_{\text{MP}} = 0.5 \text{ GeV, and } m_a = 1 \text{ GeV}. \qquad (35)$$

The magnitude of the momentum kick per collision, q_L, was found to be 0.8-1 GeV/c. The centrality dependence of the ridge yield can be described by

$$\zeta = 0.20, \;\; \sigma = 1.4 \text{ mb}, \;\; t_0 = 0.6 \text{ fm/c}. \qquad (36)$$

For the description of the jet fragments, extensive set of PHENIX data gives systematics of the jet fragments as given in Eqs. (7), (8), and (9).

In going from AA collisions at 0.2 TeV to pp collisions at 7 TeV, there are similarities and obvious differences. The plateau structure of the medium parton distributions in the two cases are expected to be similar, and the extension of the plateau should similarly depend on the beam rapidity y_B as given in Eq. (3) and (4).

We need to know the size of the proton and how the multiplicity depends on centrality. The extrapolated pp cross section at 7 TeV (PDG, 2010) gives [74],

$$\sigma_{\text{tot}}(pp) \sim 110 \text{ mb}, \; \sigma_{\text{elastic}} \sim 30 \text{ mb}. \qquad (37)$$

Therefore, the pp inelastic cross section at this energy is

$$\sigma_{\text{inel}} \sim 80 \text{ mb}. \qquad (38)$$

Sum of $p+p$ radii in a pp inelastic collision is then

$$R = \sqrt{80 \text{ mb}/\pi} = 1.59 \text{ fm} = R_A + R_B. \qquad (39)$$

Therefore, each proton has a radius $R_A = 0.8$ fm for inelastic collisions with the production of particles.

There is however an important difference between RHIC and LHC that must be taken into account. For CMS data for pp collisions at $\sqrt{s_{NN}}$=7 GeV [75],

$$\langle p_T \rangle = 0.545 \text{ GeV/c}. \tag{40}$$

For RHIC collisions at $\sqrt{s_{NN}}$ =0.2 TeV,

$$\langle p_T \rangle = 0.39 \text{ GeV/c} \tag{41}$$

Therefore, the average transverse momentum of produced medium particle at 7 TeV is enhanced from the average transverse momentum of produced medium particle at 0.2 TeV by the factor

$$\frac{\langle p_T \rangle (7 \text{ TeV})}{\langle p_T \rangle (0.2 \text{ TeV})} = \frac{0.545 \text{ GeV/c}}{0.39 \text{ GeV/c}} = 1.4. \tag{42}$$

Because of this enhancement in the average p_T values, it is necessary to scale those quantities that are related directly to transverse momentum by this empirical factor of 1.4. Accordingly, the relevant parameters that we need to change are the medium parton temperature T, the jet fragment temperature T_{JF}, and the medium parton initial time t_0 which varies roughly as $1/p_T$. For the analysis of CMS data at 7 TeV, we are well advised to scale up $T_{\rm MP}$ and T_{JF} by a factor of 1.4 to result in

$$T_{\rm MP} = 0.7 \text{ GeV}, \quad T_{JF} = 0.266 \text{ GeV } + 0.084 p_t^{\rm trig}, \tag{43}$$

and reduce the initial time t_0 by a factor of 1.4 to get
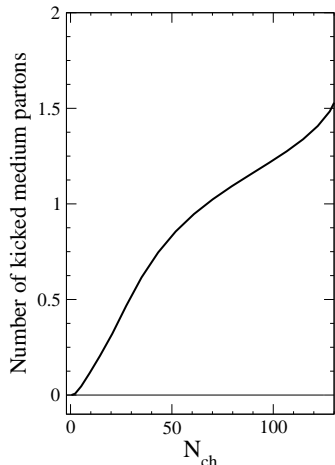
$$t_0 = 0.43 \text{ fm/c}. \tag{44}$$

FIG. 3: The number of average kicked medium partons $N_k(\boldsymbol{b})$ per trigger particle as a function of charge multiplicity $N_{\rm ch}(\boldsymbol{b})$.

As a function of the impact parameter, we calculate the average number of kicked medium partons per jet, which gives the ridge yield per jet as in Eq. (2). After calibrating the number of average droplet participants with the average number of produced charged particles as given in Eq. (30), we calculate the charge multiplicity as a function of the impact parameter. These two calculations gives the ridge yield per jet as a function of multiplicity.

The jet trajectory calculation indicates that the average number of kicked partons for the most central pp collision is about 1.5 as shown in Fig. 3. With the parameters properly scaled according to the transverse momenta, the only free parameter is q_L, the magnitude of the momentum kick acquired by the medium parton per jet-MP collision. Previously, for the STAR data at 0.2 TeV, the magnitude of q_L was found to be 0.8-1.0 GeV/c per kick. We vary q_L to fit the variation of the CMS ridge yield data in different p_T windows. If the magnitude of q_L remains at 1 GeV/c, the ridge yield will be too large in the regions of $0.1 < p_T < 1$ GeV/c and too small in the region $2 < p_T < 3$ GeV/c. The results do not agree with data. It is found that the magnitude of the kick $q_L = 2$ GeV/c gives results that are qualitatively consistent with the data. The yield per trigger particle for different regions of associated particle p_T, as a function of the multiplicity, is shown in Fig. 4 where the CMS data are shown as solid points and the momentum kick model results are shown as curves. The general trend of the experimental data is reasonably reproduced by the momentum kick model.
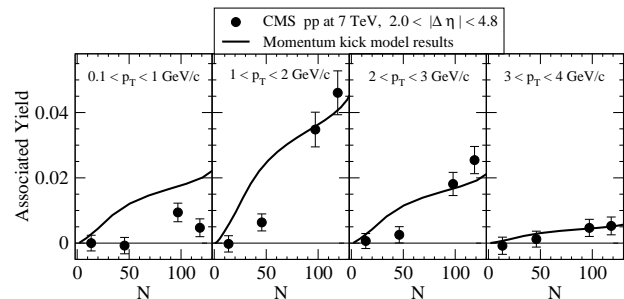

FIG. 4: The ridge yield per trigger particle for different regions of associated particle p_T, as a function of the multiplicity in the interval $2 < |\Delta\eta| < 4.8$. (a) is for $0.1 < p_T < 1$ GeV/c, (b) for $1 < p_T < 2$ GeV/c, (c) for $0.2 < p_T < 3$ GeV/c, and (d) for $3 < p_T < 4$ GeV/c.

Another indication of the dependence of the angular distribution of the associated particle yield on transverse momentum of the associated particle is shown in Fig. 5 where Fig. 5(a) is for $0.1 < p_T < 1.0$ GeV/c, and 5(b) is for $1 < p_T < 3$ GeV/c. The top of the distributions have been truncated to show the distributions in a finer scale. The ridge structure is almost imperceptible for $0.1 < p_T < 1.0$ GeV/c in Fig. 5(a) but shows up clearly for $1.0 < p_T < 3.0$ GeV/c in Fig. 5(b). The theoretical associated particle yield pattern of the $\Delta\eta$-$\Delta\phi$ angular distributions as a function of p_T agrees with those observed in CMS experiments.

To exhibit further the dependence of the ridge yield on p_t and collision energy, we note that for AuAu collisions at 0.2 TeV within the acceptance windows of the STAR Collaboration, yields from the jet fragments and the ridge component have been measured experimentally.
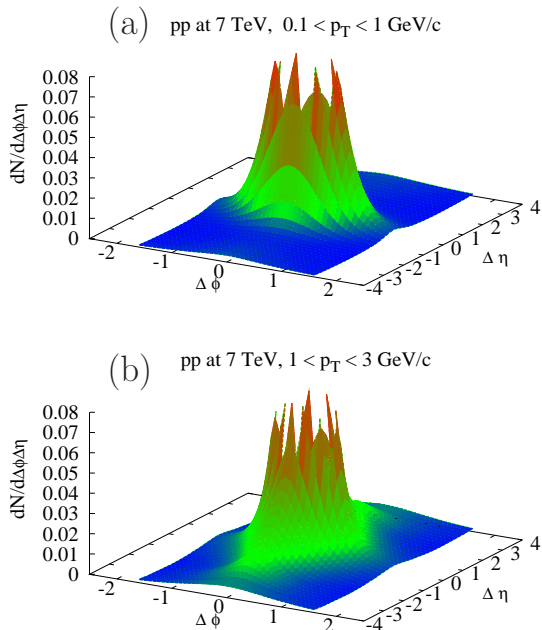
FIG. 5: (Color online) The distribution of associated particles for *pp* collisions at 7 TeV calculated in the momentum kick model. The peaks of the distributions have been truncated at the top. Fig. 4 (a) is for $0.1 < p_T < 1$ GeV/c and Fig. 4 (b) is for $1 < p_T < 2$ GeV/c.

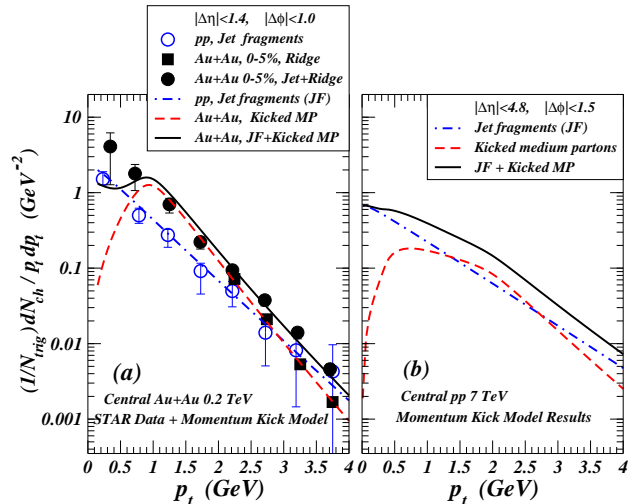NJF-NJF yields as p_T increases above 3 GeV/c.

FIG. 6: (Color online) (a) The p_T distribution of associated particles for AuAu collisions at 0.2 TeV as a function of p_T. the curves are momentum kick model results and the data points are from the STAR Collaboration. (b) The p_T distribution of associated particles obtained in the momentum kick model for *pp* collisions at 0.2 TeV.

The data points are given in Fig. 6(a). The different components have been successfully separated and interpreted in the momentum kick model, as shown in Fig. 6(a) where the theoretical results are shown as curves. One observes in Fig. 6(a) that the ridge yield $dN_{ch}/N_{trig}p_T dp_T$ has a peak at about 1 GeV/c, which is about the same as the magnitude of the momentum kick $q_L = 1$ GeV/c. Because $T_{MP} < T_{JF}$, the NJF-NJF component dominates over the NJF-NKMP components at large p_T.

To make meaningful comparison with *pp* collisions at 7 TeV, we calculate $dN_{ch}/N_{trig}p_T dp_T$ in the momentum kick model with $q_L = 2$ GeV/c within the CMS experimental windows with a $p_T > 5$ GeV/c trigger. The theoretical results are shown as curves in Fig. 6(b). The ridge yield distributions are the medium parton distributions displaced by the momentum kick along the jet direction. As a consequence, the peak of the ridge yield moves to a larger value of p_T and becomes broader over a large region between 0.5 to 2.5 GeV/c for *pp* collisions at 7 TeV with $q_L = 2$ GeV/c. The large pseudorapidity window for the trigger jet enhances the broadening of the peak of the distribution for *pp* collisions. These theoretical results explain why the associated particle yield is distributed more in the region of $1 < p_T < 3$ GeV/c than in other regions in *pp* collisions at 7 TeV. Note again that because the the higher temperature for the NJF-NJF component, the ridge yield become smaller than the

VI. CONCLUSIONS AND DISCUSSIONS

The CMS observation of the ridge structures in *pp* collisions at 7 TeV raises many interesting questions which we can try to answer in the momentum kick model. We find that in *AA* as well as in *pp* collisions, the ridge arises from the medium partons that are kicked by the jet and they acquire a momentum kick along the jet direction. Because the collision occurs at the early stage in the presence of the jet, the ridge provides direct information on the momentum distribution of the medium partons at the moment of jet-(medium parton) collision.

The STAR, PHENIX, and PHOBOS data for *AA* collisions at RHIC and the CMS data for *pp* collisions at LHC are consistent with the initial momentum distributions in the form of a rapidity plateau, with a thermal like transverse momentum distribution. While the functional form of the momentum distribution is the same, the longitudinal and transverse momentum at the two energies need to be properly scaled according the their differences in collision energies. The longitudinal rapidity need to be scaled according to the collider beam rapidity y_B in the center-of-mass system, and the transverse momentum distribution temperature parameters for *pp* collision at 7 TeV need to be scaled up by a factor of 1.4 compared to the case of 0.2 TeV, and the medium particle initial time t_0 reduced by the same factor of 1.4. This factor of 1.4 was estimated from the ratio of the average transverse momenta of *pp* collisions at the two different energies.

We estimate that the average number of kicked medium partons in the most central pp collisions at 7 TeV with the highest multiplicity is approximately 1.5. This is less than the number of kicked medium partons of about 4 for the most central Au-Au collisions at 0.2 TeV. The medium produced in pp collision at 7 TeV is not as dense as the medium produced in the most central AuAu collisions at 0.2 TeV, but the medium is nonetheless dense enough for the jet to kick the medium partons to turn them into ridge particles for our examination.

Using our knowledge of the physical quantities in the momentum kick model analyses for AA collisions at RHIC energies, there is only a single parameter we vary in trying to understand pp data at 7 TeV. We find that in pp collisions at 7 TeV, experimental data suggest a greater momentum kick value, $q_L = 2$ GeV/c, which is twice as large as $q_L \sim 1$ GeV/c for RHIC AA collisions at 0.2 TeV.

The ridge yields for pp collisions are more prominent in the region of $1 < p_T < 3$ GeV/c. Such a feature arises because the ridge particles are just particles whose momenta are shifted by the momentum kick. The shift of $q_L = 2$ GeV/c will place the center of the momentum distribution in the p_T region between 1 and 3 GeV/c region. Hence the ridge yield is greater in this region compared to other p_T regions.

The approximate validity of the momentum kick model raises the interesting question on the nature of the scattering between the jet and the medium partons. It suggests a picture of the medium parton absorbing a part of the jet longitudinal momentum in its scattering with the jet. We can envisage that the jet at this stage is a transversely broad object in the form of a cloud of gluons propagating together in a bundle, and the complete absorption of a part of the gluon cloud by the medium parton imparts the longitudinal momentum to the medium parton to carry the medium parton out to become a ridge particle. In this simple description, the jet behaves like a composite object and the scattering between the jet and the medium is not a simple two-body scattering process, as in the case with a jet parton of ultra-high p_T. It is more like "shooting a water hose on a bunch of fast-moving ping-pong balls" [76]. Further theoretical and experimental investigations on the nature of the jet-(medium parton) collision for relatively low-p_T jets at this stage will be of great interest.

Transverse hydrodynamical expansion will lead to azimuthal correlations [32, 33, 40, 41, 49–51]. However, a quantitative analysis of the effects of the dynamical expansion needs to be examined carefully as the transverse flow depends sensitively on time [65] and it is much slower than the longitudinal expansion [66]. Furthermore, the transverse hydrodynamics for a fluid system with non-isotropic momentum distribution in the early history of the expansion has not been worked out in details. In the analogous case with an isotropically thermalized fluid, the picture of transverse expansion [65] reveals that soon after the stage of transverse overlap at which the jets are produced, the medium is essentially at rest with little transverse expansion. The transverse expansion commences only after the rarefaction wave passes through the medium from the outer surface inward. The time for the rarefaction waves to travel depends on the radius of the medium and the speed of the rarefaction wave which is the speed of sound. Future investigations on hydrodynamical solutions for a non-isotropic momentum distributions and azimuthally asymmetric shapes will provide a more accurate calculation of the effects of transverse flow in azimuthal correlations.

Whatever the proposed mechanism may be, collisions of the jet with the medium partons are bound to occur, and the collisional correlation between the colliding objects as discussed in the momentum kick model must be taken into account because these collisional correlations will contribute to the two-particle correlation function.

The momentum kick model provides a unifying description for ridges with or without a high-p_T trigger. The description generalizes the trigger to include high-p_T and low-p_T particles owing to the fact that jet fragments are found in high p_T as well as in low p_T. If we limit our attention to the near-side, the case with a high-p_T trigger involves mainly NJF-NJF and NJF-NKMP correlations while the case of autocorrelations with low-p_T particles involves not only these NJF-NJF and NJF-NKMP correlations but also the NKMP-NKMP correlation. The additional NKMP-NKMP correlation in the low-p_T trigger case will contribute only when more than one medium partons are kicked by the same jet and will be important in the ridge region. In extended dense medium as occurs in heavy-ion collisions, the number of partons kicked by the same jet becomes considerable and this NKMP-NKMP contribution should be appropriately taken into account. However, in pp collisions, the number of medium partons kicked by the same jet on the near-side is small, the NKMP-NKMP contribution is small in comparison with the other NJF-NJF and NJF-NKMP contributions, and can be approximately neglected in near-side correlation analysis.

In conclusion, the ridges in both AA collisions at 0.2 TeV and pp collisions at 7 TeV in LHC can be described by the same mechanism of the momentum kick model involving the collision of jets with medium partons. The momentum distributions of the medium partons at the moment of jet-(medium parton collision) have similar features of a rapidity plateau and a thermal type transverse momentum distribution.

Future experiments call for the acquisition of more data of the ridge yields in a large regions of the phase space in different phase space cuts and combinations so that the momentum distribution can be more precisely determined.

[1] CMS Collaboration, JHEP 1009, 091 (2010),[arXiv:1009.4122].
[2] CMS Collaboration, arXiv:1105.2438 (2011).
[3] J. Adams *et al*. for the STAR Collaboration, Phys. Rev. Lett. **95**, 152301 (2005);
[4] J. Adams *et al*. (STAR Collaboration), Phys. Rev. C **73**, 064907 (2006).
[5] J. Putschke (STAR Collaboration), J. Phys. **G34**, S679 (2007).
[6] J. Bielcikova (STAR Collaboration), J. Phys. **G34**, S929 (2007).
[7] F. Wang (STAR Collaboration), Invited talk at the XIth International Workshop on Correlation and Fluctuation in Multiparticle Production, Hangzhou, China, November 2007, [arXiv:0707.0815].
[8] J. Bielcikova (STAR Collaboration), Phys.G34:S929-930,2007; J. Bielcikova for the STAR Collaboration, Talk presented at 23rd Winter Workshop on Nuclear Dynamics, Big Sky, Montana, USA, February 11-18, 2007, [arXiv:0707.3100]; J. Bielcikova for the STAR Collaboration, Talk presented at XLIII Rencontres de Moriond, QCD and High Energy Interactions, La Thuile, March 8-15, 2008, [arXiv:0806.2261].
[9] B. Abelev (STAR Collaboration), Talk presented at 23rd Winter Workshop on Nuclear Dynamics, Big Sky, Montana, USA, February 11-18, 2007, [arXiv:0705.3371].
[10] L. Molnar (STAR Collaboration), J. Phys. G **34**, S593 (2007).
[11] R. S. Longacre (STAR Collaboration), Int. J. Mod. Phys. E**16**, 2149 (2007).
[12] C. Nattrass (STAR Collaboration), J. Phys. G **35**, 104110 (2008).
[13] A. Feng, (STAR Collaboration), J. Phys. G **35**, 104082 (2008).
[14] P. K. Netrakanti (STAR Collaboration) J. Phys. G **35**, 104010 (2008).
[15] O. Barannikova (STAR Collaboration), J. Phys. G **35**, 104086 (2008).
[16] M. Daugherity, (STAR Collaboration), J. Phys. G **35**, 104090 (2008).
[17] M. van Leeuwen, (STAR Collaboration), Eur. Phys. J. C **61**, 569 (2009).
[18] A. Adare, *et al*. (PHENIX Collaboration), Phys. Rev. C **78**, 014901 (2008).
[19] M. P. McCumber (PHENIX Collaboration), J. Phys. G **35**, 104081 (2008).
[20] Chin-Hao Chen (PHENIX Collaboration), "Studying the Medium Response by Two Particle Correlations", Hard Probes 2008 Intern. Conf. on Hard Probes of High Energy Nuclear Collisions, A Toxa, Galicia, Spain, June 8-14, 2008.
[21] Jiangyong Jia, (PHENIX Collaboration), J. Phys. G **35**, 104033 (2008).
[22] M.J. Tannenbaum, Eur. Phys. J. C **61**, 747 (2009).
[23] E. Wenger (PHOBOS Collaboration), J. Phys. G **35**, 104080 (2008).
[24] T. A. Trainor and D. T. Kettler, Phys. Rev. D 74, 034012 (2006); T. A. Trainor, Phys. Rev. C 80, 044901 (2009);T. A. Trainor, J. Phys. G 37, 085004 (2010).
[25] C. Y. Wong, Phys. Rev. C **76**, 054908 (2007).
[26] C. Y. Wong, Chin. Phys. Lett. **25**, 3936 (2008)
[27] C. Y. Wong, J. Phys. G **35**, 104085 (2008).
[28] C. Y. Wong, Phys. Rev. C **78**, 064905 (2008).
[29] C. Y. Wong, Phys. Rev. C **80**, 034908 (2009).
[30] C. Y. Wong, Phys. Rev. C **80**, 054917 (2009).
[31] C.-Y. Wong, Nonlin. Phenom. Complex Syst. **12**, 315 (2009), [arXiv:0911.3583]
[32] E. Shuryak, Phys. Rec. C **76**, 047901 (2007).
[33] S. A. Voloshin, Nucl. Phys. **A749**, 287 (2005).
[34] C. B. Chiu and R. C. Hwa Phys. Rev. C **79**, 034901 (2009).
[35] R. C. Hwa and C. B. Yang, Phys.Rev. C **67** 034902 (2003); R. C. Hwa and Z. G. Tan, Phys. Rev. C **72**, 057902 (2005); R. C. Hwa and C. B. Yang, [nucl-th/0602024].
[36] C. B. Chiu and R. C. Hwa Phys. Rev. C **72**, 034903 (2005).
[37] R. C. Hwa, [arXiv0708.1508].
[38] V. S. Pantuev, [arXiv:0710.1882].
[39] A. Dumitru, F. Gelis, L. McLerran, and R. Venugopalan, Nucl. Phys. A**810**, 91 (2008).
[40] S. Gavin, and G. Moschelli, J. Phys. G **35**, 104084 (2008).
[41] S. Gavin, L. McLerran, and G. Moschelli, Phys. Rev. C **79**, 051902 (2009).
[42] N. Armesto, C. A. Salgado, U. A. Wiedemann, Phys. Rev. Lett. **93**, 242301 (2004).
[43] P. Romatschke, Phys. Rev. C **75** 014901 (2007).
[44] A. Majumder, B. Muller, and S. A. Bass, Phys. Rev. Lett. **99**, 042301 (2007).
[45] A. Dumitru, Y. Nara, B. Schenke, and M. Strickland, Phys. Rev. C **78**, 024909 (2008); B. Schenke, A. Dumitru, Y. Nara, M. Strickland, J. Phys. G **35**, 104109 (2008).
[46] R. Mizukawa, T. Hirano, M. Isse, Y. Nara, and A. Ohnishi, J. Phys. G **35**, 104083 (2008).
[47] Jianyong Jia and R.. Lacey, Phys. Rev. C **79**, 011901 (2009).
[48] Jianyong Jia, Eur. Phys. J. C **61**, 255 (2009).
[49] Y. Hama, R. P. G. Andrade, F. Grassi, W.-L. Qian, Talk presented at ISMD2010, 21-25 September, 2010, University of Antwerp (Belgium), [arXiv:1012.1342].
[50] A. Dumitru, K. Dusling, F. Gelis, J. Jalilian-Marian, T. Lappi, R. Venugopalan Phys. Lett. **B697** 21 (2011), [arXiv:1009.5295].
[51] K. Werner, Iu. Karpenko, K. Mikhailov, and T. Pierog [arXiv:1104.3269].
[52] R. C. Hwa, C. B. Yang, Phys. Rev. **C 83**, 024911 (2011), [arXiv:1011.0965].
[53] C. B. Chiu and R. C. Hwa, [axriv:1012:3485]
[54] T. A. Trainor, arXiv:1008.4757; T. A. Trainor, arXiv:1011.6351; T. A. Trainor, arXiv:1012.2373.
[55] Thomas A. Trainor, David T. Kettler arXiv:1010.3048.
[56] B. A. Arbuzov, E. E. Boos, V. I. Savrin, arXiv:1104.1283.
[57] M.Yu. Azarkin, I.M. Dremin, A.V. Leonidov, arXiv:1102.3258.
[58] H. R. Grigoryan, Yuri V. Kovchegov arXiv:1012.5431,
[59] I. Bautista, J. Dias de Deus, C. Pajares, arXiv:1011.1870.
[60] I.O. Cherednikov, N.G. Stefanis, arXiv:1010.4463.
[61] Igor M. Dremin, Victor T. Kim, arXiv:1010.0918.
[62] E. Levin, A. H. Rezaeian arXiv:1105.3275.
[63] C. Y. Wong, *Introduction to High-Energy Heavy-Ion Collisions*, World Scientific Publishing Company, 1994.
[64] T. T. Chou and C. N. Yang, Phys. Rev. 170, 1591 (1968);

T. T. Chou and C. N. Yang, Phys. Lett. B 135, 175 (1984).

[65] G. Baym, B. L. Friman, J.-P. Blaizot, M. Soyeur, and W. Czyz, Nucl. Phys. **A407**, 541 (1983).

[66] L. D. Landau, Izv. Akad. Nauk SSSR **17**, 51 (1953); S. Z. Belenkij and L. D. Landau, Usp. Fiz. Nauk **56**, 309 (1955); Nuovo Cimento, Suppl. **3**, 15 (1956).

[67] C. Y. Wong, Phys. Rev. C **78**, 054902 (2008).

[68] C. Y. Wong, Lectures presented at the Helmholtz International Summer School, Bogoliubov Laboratory of Theoretical Physics, JINR, Dubna, July 14-26, 2008, [arXiv:0809.0517].

[69] M. Basile *et al.*, Nuovo Cim. **65A**, 400 (1981); M. Basile, Nuovo Cim. **67A**, 244 (1981).

[70] U. W. Heinz and P. F. Kolb, Nucl. Phys. **A702**, 269 (2002).

[71] A. Casher, J. Kogut, and L. Susskind, Phys. Rev. D **10**, 732 (1974).

[72] J. D. Bjorken, Phys. Rev. D **27**, 140 (1983).

[73] C. Y. Wong, R. C. Wang, and C. C. Shih, Phys. Rev. D **44**, 257 (1991).

[74] K. Nakamura et al. (Particle Data Group), J. Phys. G 37, 075021 (2010)

[75] V. Khachatryan *et al.*, CMS Collaboration, Phys. Rev. Lett. **105**, 022002 (2010).

[76] The author thanks Denny Ray for such a colorful description of the momentum kick model.